Communications in Physics, Vol. 33, No. 4 (2023), pp. 421-433
DOI: https://doi.org/10.15625/0868-3166/18859

H_2 adsorption isotherms of Mg-MOF-74 isoreticulars: An integrated approach utilizing a thermochemical model and density functional theory

Thuy-Trang Nguyen[1,2,†], **Cao Cong-Phuong**[1], **Phong Le-Hoang**[1], **Linh Nguyen-Hoang**[3], **Nam Vu-Hoang**[2], **Toan Nguyen The**[1] **and Thang Phan Bach**[2]

[1]*Key Laboratory for Multiscale Simulation of Complex Systems, University of Science, Vietnam National University – Hanoi, Hanoi, Vietnam*

[2]*Center for Innovative Materials and Architectures, Vietnam National University Ho Chi Minh city, Ho Chi Minh City, Vietnam*

[3]*School of engineering physics, Hanoi University of Technology, Hanoi, Vietnam*

E-mail: [†]nguyenthuytrang@hus.edu.vn

Received 12 September 2023; *Accepted for publication 3 October 2023*
Published 8 December 2023

Abstract. *A thermochemical model was developed to calculate the H_2 adsorption isotherm of the original Mg-MOF-74 framework, and its computationally designed isoreticular employing the adsorption energies and vibrational frequencies obtained from density functional theory calculations as input variables. The model reasonably replicates the experimental adsorption isotherm of the original framework at -196˚C within the pressure range up to 1 bar. The strongest adsorption site of the new Mg-MOF-74 isoreticular exhibits saturation at lower pressure compared to the original one, despite a lower adsorption energy. This emphasizes the importance of vibrational, rotational, and translational contributions for comprehensively assessing the site's adsorption performance. Because only the strongest adsorption site was taken into account for the site-site interaction, the model is only valid for low coverage rates of secondary sites. Consequently, it strongly overestimates the hydrogen uptake of the original isoreticular at higher temperature and pressure ranges where the cumulative coverage rate of the secondary adsorption sites is comparable to that of the strongest sites. In contrast, the model remains valid for the new isoreticular at a specific temperature between -40˚C and 60˚C within the pressure range up to 25 bar where the coverage rate of the secondary adsorption site is low. Its predictions highlights the significantly improved performance of the new framework compared to the original framework. Specially, it achieves a gravimetric hydrogen uptake value between 2.8 wt% and 1.9 wt% at a pressure of 25 bar within the mentioned temperature swing which is substantially higher than that of the original framework.*

Keywords: Hydrogen physisorption; metal organic framework; hydrogen adsorption isotherm.
Classification numbers: 68.03.-g; 84.60.Ve; 81.05.Lg; 81.05.Rm; 81.05.Zx.

1. Introduction

Solid-state hydrogen storage offers a promising solution for effectively incorporating renewable energy into mobile applications [1]. The core focus of this technology resolves around solid materials that are able to facilitate the diffusion of hydrogen into their structures, thereby stabilizing it in either atomic or H_2 molecular forms [2]. This allows the compacting of hydrogen at high densities while maintaining sustainable pressure. Extensive ongoing research has been being dedicated to identifying hydrogen storage materials that align with the objectives set up by the United States Department of Energy (DOE) for mobile applications. In particular, the ultimate target of on-board hydrogen storage in light-duty fuel cell vehicle is 7.5 wt.% hydrogen and 70 g hydrogen/L within the temperature range of -40˚C to 60˚C, with the delivery temperature ranging from -40˚C and 80˚C [3].

On the base of the host-guest interaction, hydrogen storage materials in current trends can be classified into chemisorption and physisorption materials [1]. Chemisorption materials including metal hydrides, metal borohydrides and complex hydrides possess a great advantage in that they inherently consist of hydrogen atoms in their chemical compositions, resulting in hydrogen densities that consistently exceeds the DOE target [4]. However, the development of chemisorption-based storage techniques faces several challenges. These include complicated desorption processes that require high temperatures ranging from 200˚C to 600˚C [5–7], as well as slow charge-discharge processes due to the inherent high activation energy required for chemical bond formation [8, 9]. In contrast, physisorption materials are porous substances such as zeolite [10], carbon based materials [11–16], covalence organic frameworks (COFs) [17–20] and metal organic frameworks (MOFs) [21]. They are able to facilitate the diffusion of H_2 molecules into their pores, where they become attached to the pore surfaces through barrierless physical attractions such as Van der Waals and electrostatic interactions [10–21]. These materials offer the advantage of fast charge-discharge processes due to the reversibility of physical adsorption [22, 23]. However, the weak physical attractions, typically with strengths ranging from 5 to 10 kJ/mol, limit the usable uptake of hydrogen under extreme conditions, such as at liquid nitrogen temperatures (77 K) and/or high pressures [24–26].

While the host-guest binding strength, typically measured by the adsorption energy, serves as an important parameter for evaluating the potential of a physisorption material to meet DOE targets, there is no straightforward method to derive the adsorption isotherm from the adsorption energy. The traditional approach commonly used to calculate the adsorption isotherm is classical force-field-based Grand Canonical Monte Carlo (GCMC) simulation [27–29]. However, this method does not directly derive the adsorption isotherm from the adsorption energy. It heavily relies on carefully constructing and benchmarking the classical force field using experimental data and density functional theory (DFT) output to properly describe the host-guest interactions. A GCMC simulation using a poorly parameterized force field would fail to reproduce the experimental adsorption isotherm [27].

The objective of this work is to derive the H_2 adsorption isotherm of two MOF isoreticulars directly from the adsorption energies and vibrational frequencies predicted by the DFT method, employing a simple thermochemical model. The two MOF isoreticulars considered are the original Mg-MOF-74 framework, based on an aromatic benzene dicarboxylate (BDC) linker (BDC-Mg-MOF-74) and its computationally designed variant, based on nonaromatic dihydroxyfumate

(DHF) linker (DHF-Mg-MOF-74) [27]. We replicate the experimental H_2 adsorption isotherm of the original BDC-Mg-MOF-74 framework at -196˚C, within the pressure range of up to 1 bar. Furthermore, we predicted the adsorption isotherm of the newly designed DHF-Mg-MOF-74 framework under various pressure and temperature conditions. These predictions indicate that the new framework exhibits significantly enhanced H_2 adsorption performance compared to the original framework.

2. Methods and computational details

2.1. H_2 adsorption sites on the internal surface of MOF-74 isoreticulars

The MOF-74 family possesses a well-defined crystalline structure with a rhombohedral lattice (Fig. 1a). It consists of one-dimensional (1D) chains comprised of edge-sharing MO_5 pyramids, where M represents metals such as Mg, Fe, Mn, Co and Ni (Fig. 1b). These chains align along the *c* direction and are interconnected by organic linkers, forming a honeycomb network within the *ab* plane. This unique structure gives rise to the porosity of the material, characterized by void channels that run along the *c* direction. In this study, two Mg-MOF-74 isoreticulars are investigated, namely the original Mg-MOF-74 framework based on aromatic benzenedicarboxylate (BDC) linker and the computationally designed variant based on nonaromatic dihydroxyfumate (DHF) linker (Fig. 1c) [27].

In our previous work, *ab initio* molecular dynamics (AIMD) simulations successfully replicated four distinct types of adsorption sites on the internal surface of the original BDC-Mg-MOF-74 framework (Fig. 1d) [30]. The strongest adsorption sites were found nearest to the OMSs and denoted as PM. The remaining sites, arranged in descending order of binding strength, were found closest to the oxygen atoms of the oxido groups (PO1), aromatic rings (PR) and the oxgen atoms of the carboxyl groups (PO2), respectively. In contrast, the AIMD simulation exhibited only two types of adsorption sites in the internal surface of the newly-proposed DHF-Mg-MOF-74 framework (Fig. 1e). The strongest sites were still the ones nearest to the OMSs (PM), while the other sites were in proximity to the oxygen atoms of carboxyl groups (PO2). The absence of the sites belonging to the other two types can be attributed to the shorter length and nonaromatic nature of the DHF linker in comparison to the BDC linker.

2.2. Multiple-site Langmuir model of adsorption

The original Langmuir adsorption model, introduced by Irving Langmuir, is the simplest model to describe the relationship between the surface coverage rate of an adsorbed gas θ and the pressure of the gas on the surface P at a specific temperature T [31]. It is based on the following key assumptions:

(1) All adsorption sites have equal adsorption energies, meaning there is only one type of adsorption sites.
(2) Each site can only accommodate a single molecule, forming a monolayer on the surface.
(3) There is no interaction between molecules on adjacent sites, implying that the adsorption energy does not depend on coverage rate.

In order to determine the surface coverage rate $\theta(T,P)$, the adsorption process is considered as an equilibrium where the rate of gas molecules being adsorbed onto the surface is balanced by the

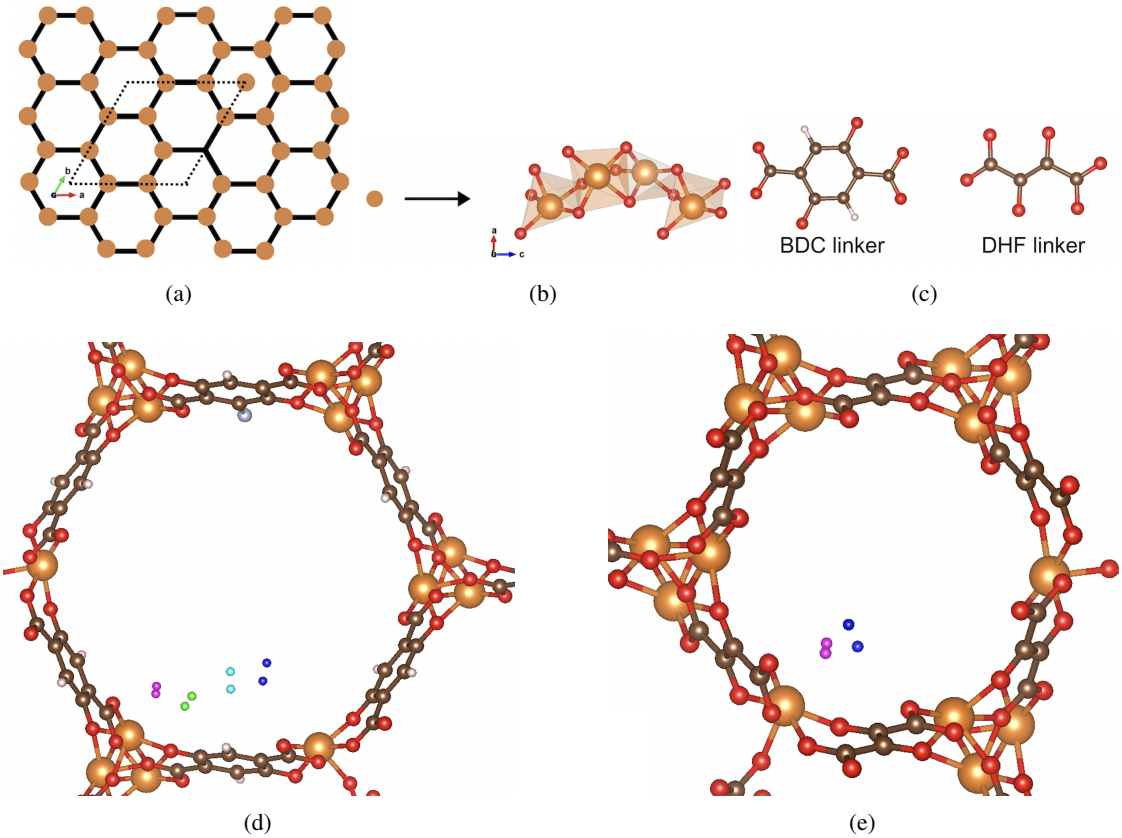

Fig. 1. (a) Rhombohedral lattice of MOF-74 family viewed along c direction. Orange rounds represent one-dimensional (1D) chains comprised of edge-sharing MO_5 pyramids (M= Mg, Fe, Mn, Co and Ni). Black solid lines represent organic linkers that connect pyramid chains forming honeycomb lattice in ab plane. Black dot lines represent a rhombohedral unit cell. (b) A segment of a one-dimensional (1D) chain comprised of edge-sharing MO_5 pyramids. Orange and red spheres represent metal and oxygen atoms respectively. Pyramids are represented by opaque orange color. (c) The aromatic benzenedicarboxylate (BDC) (left) and nonaromatic dihydroxyfumate (DHF) linker (right). Red, brown and white spheres represent oxygen, carbon and hydrogen atoms respectively. (d) Adsorption positions of various types on the internal surface of the BDC-Mg-MOF-74 and (e) DHF-Mg-MOF-74. Red, brown and white spheres represent oxygen, carbon and hydrogen atoms respectively. Pink, green, cyan and blue colors denote H_2 molecules adsorbed at PM, PO1, PR and PO2 respectively.

rate of molecules desorbing back into the gas phase. Consequently, the coverage rate is expressed as:

$$\theta(T,P) = \frac{\frac{P}{P_0}\exp\left(-\frac{\Delta G}{RT}\right)}{1+\frac{P}{P_0}\exp\left(-\frac{\Delta G}{RT}\right)}, \tag{1}$$

where ΔG represents the Gibbs free energy of adsorption; R is the ideal gas constant and P_0 denotes the standard pressure $P_0 = 1$ atm.

The first assumption of the original Langmuir model is not applicable when studying H_2 adsorption on the internal surface of MOF-74 isoreticulars because of the presence of multiple adsorption sites with varying adsorption energies. Therefore, a multiple-site model is formulated based on the original single-site Langmuir model. The first step involves treating each site independently using the single-site formula to obtain the initial site-specific coverage rates:

$$\theta_s(T,P) = \frac{\frac{P}{P_0}\exp\left(-\frac{\Delta G_s}{RT}\right)}{1+\frac{P}{P_0}\exp\left(-\frac{\Delta G_s}{RT}\right)}. \tag{2}$$

Here, the index s represents the type of adsorption site, i. e. s = PM, PO1, PR and PO2 for the BDC-MOF-74 framework and s = PM and PO2 for the DHF-MOF-74 framework. ΔG_s is the enthalpy of adsorption of that particular site. Next, the overall surface coverage rate $\theta(T,P)$ is calculated as follows:

$$\theta(T,P) = \sum_s \chi_s \theta_s(T,P). \tag{3}$$

In this equation, χ_s is the weight of site s, which is the ratio of the number of sites s to the total number of adsorption sites. There are four types of adsorption sites on the internal surface of the BDC-MOF-74 framework, with an equal weight of 0.25 for all types. For the DHF-MOF-74 framework, there are two types with an equal weight of 0.5.

The site-site interactions should be taken into account to make the model more practical. This means that the adsorption energies will no longer remain constant but would instead depend on the coverage rates $\Delta G_s(\theta)$. For simplicity, we assume that within the pressure range below 1 bar, only the coverage rate of the strongest adsorption sites, θ_{PM} is high enough to affect the adsorption energies significantly. The dependence can be approximately linearly expressed as:

$$\Delta G_s(\theta_{PM}) = \Delta G_s(\theta_{PM}=0) + \theta_{PM}[\Delta G_s(\theta_{PM}=1) - \Delta G_s(\theta_{PM}=0)]. \tag{4}$$

Here, $\Delta G_s(\theta_{PM}=0)$ represents the Gibbs free energy of adsorption when a gas molecule is adsorbed at the position i on an empty surface, while $\Delta G_s(\theta_{PM}=1)$ represents the Gibbs free energy of adsorption when the strongest sites are fully occupied. Finally we have a set of equations (2) and (4) which can be solve iteratively with $\Delta G_s(\theta_{PM}=0)$ and $\Delta G_s(\theta_{PM}=1)$ calculated from the output of DFT calculations as described below.

2.3. Gibbs free energy from the outputs of DFT calculations

It is well-known from textbook that the Gibbs free energy of a molecular system can be calculated in terms of partition functions:

$$G = -k_B T(\ln Q_e + \ln Q_{vib}) + \ln Q_{rot} + \ln Q_{trans} + PV, \tag{5}$$

where Q_e, Q_{vib}, Q_{rot} and Q_{trans} are electronic, vibrational, rotational and translational partition functions, respectively [32]. Considering that the electronic energy gap of MOF-74, E_{gap} is approximately 2 eV [33], resulting in negligibly small Boltzmann population ratio $\frac{E_{gap}}{k_B T} \approx 10^{-34}$ at room temperature, the electronic part of the Gibbs free energy can be approximated as the zero-temperature electronic energy calculated from static DFT calculations E. Thus, we have:

$$G = E - k_B T(\ln Q_{vib} + \ln Q_{rot} + \ln Q_{trans}) + PV = E + A_{vib} + \ln Q_{trans} + PV. \tag{6}$$

The Gibbs free energy of adsorption is defined as:

$$\begin{aligned}\Delta G =& G_{fr+\mathrm{H_2}} - G_{fr} - G_{\mathrm{H_2}} \\ =& E_{fr+\mathrm{H_2}} - E_{fr} - E_{\mathrm{H_2}} + \left(A_{vib}^{fr+\mathrm{H_2}} + A_{rot}^{fr+\mathrm{H_2}} + A_{trans}^{fr+\mathrm{H_2}}\right) \\ & - \left(A_{vib}^{fr} + A_{rot}^{fr} + A_{trans}^{fr}\right) - \left(A_{vib}^{\mathrm{H_2}} + A_{rot}^{\mathrm{H_2}} + A_{trans}^{\mathrm{H_2}}\right).\end{aligned} \tag{7}$$

The indices $fr+\mathrm{H_2}$, fr and $\mathrm{H_2}$ denote the combined systems of $\mathrm{H_2}$ and MOF-74, bare MOF-74 frameworks and an isolated $\mathrm{H_2}$ molecule respectively. This expression can be simplified based on the following considerations. The frameworks do not undergo any rotational or translational motion. Similarly, when the $\mathrm{H_2}$ molecule is adsorbed onto the internal surface of the frameworks, it also does not undergo any rotational or translation motion. Therefore, $A_{rot}^{fr+\mathrm{H_2}}$, $A_{trans}^{fr+\mathrm{H_2}}$, A_{rot}^{fr} and A_{trans}^{fr} can be omitted. Additionally, we assume that the physical binding between the frameworks and $\mathrm{H_2}$ molecules does not significantly affect the vibrational modes of the framework. Actually, previous studies have shown that the contribution of the framework vibrations to the zero-point vibrational energy (ZPE) correction for the adsorption energy is less than 2 meV ($\approx 2\%$) [30]. Hence, A_{vib}^{fr} can be omitted and $A_{vib}^{fr+\mathrm{H_2}}$ can be approximated as that of adsorbed $\mathrm{H_2}$ molecule, presented by $A_{vib}^{adsorbed\,\mathrm{H_2}}$ and we have:

$$\begin{aligned}\Delta G =& E_{fr+\mathrm{H_2}} - E_{fr} - E_{\mathrm{H_2}} + A_{vib}^{adsorbed:\mathrm{H_2}} - \left(A_{vib}^{\mathrm{H_2}} + A_{rot}^{\mathrm{H_2}} + A_{trans}^{\mathrm{H_2}}\right) - PV \\ G =& \Delta E - k_B T \ln Q_{vib}^{adsorbed:\mathrm{H_2}} + k_B T \ln\left(Q_{vib}^{\mathrm{H_2}} Q_{rot}^{\mathrm{H_2}} Q_{trans}^{\mathrm{H_2}}\right) - PV.\end{aligned} \tag{8}$$

For 1 mole of $\mathrm{H_2}$, taking into account the following approximations and considerations:

(1) Stirling approximation: $\ln(N_A!) \approx N_A \ln N_A - N_A$;
(2) Free $\mathrm{H_2}$ gas follow ideal gas equation: $PV = N_A k_B T = RT$;
(3) The isolated $\mathrm{H_2}$ molecule is a diatomic molecule of which the translational and rotational partition function are well-known [32].

we arrive at the following expression:

$$\begin{aligned}\Delta G =& \Delta E - RT \sum_{i=1}^{6} \left\{ \frac{\hbar w_i^{adsorbed\mathrm{H_2}}}{2k_B T} + \ln\left[1 - \exp\left(\frac{-\hbar w_i^{adsorbed\mathrm{H_2}}}{k_B T}\right)\right]\right\} \\ & + RT \left\{ \frac{\hbar w_{stretching}^{\mathrm{H_2}}}{2k_B T} + \ln\left[1 - \exp\left(\frac{-\hbar w_{stretching}^{\mathrm{H_2}}}{k_B T}\right)\right]\right\} \\ & + RT \left\{ \ln\left(\frac{2\pi m_{\mathrm{H_2}} k_B T}{\hbar^2}\right)^{\frac{3}{2}} \frac{k_B T}{P} + \ln\left(\frac{1}{2}\frac{8\pi^2 I_{\mathrm{H_2}} k_B T}{\hbar^2}\right)\right\}.\end{aligned} \tag{9}$$

In this expression, R, $\hbar$ and $I_{\mathrm{H_2}}$ is the ideal gas constant, the Planck constant and moment of inertia of the $\mathrm{H_2}$ molecule respectively. ΔE, $w_i^{absorbed\,\mathrm{H_2}}$ and $w_{stretching}^{\mathrm{H_2}}$ represent the electronic term of adsorption energy, vibrational frequencies of adsorbed and free $\mathrm{H_2}$, respectively. These quantities can be calculated using DFT-D3 method as detailed below [34].

DFT calculations were performed using the *Vienna ab initio simulation package* (VASP) [35, 36]. The exchange correlation potentials were described within the generalized gradient approximation (GGA) using the PBE functional formulated by Perdew *et al* [37]. The dispersion interaction was taken into account using a method called DFT-D3 in which a dispersion correction formulated by S. Grimme was added to the Kohn-Sham equation *et al* [38]. The valence electrons' wave functions were represented in a plane wave basis set with a cutoff energy $E_{cut-off} = 550$ eV. The highly oscillating parts were represented using the projector augmented wave (PAW) method [36, 38]. Since both the BDC-based and DHF-based Mg-MOF-74 frameworks have large unit cells (sizes of $26.08 \times 26.08 \times 6.87$ Å^3 and $18.76 \times 18.76 \times 6.87$ Å^3, respectively), total energies were calculated on a $1 \times 1 \times 3$ Monkhorst-Pack mesh in reciprocal space. The self-consistent-field (SCF) convergence criterion of 10^{-6} eV was used for electronic structure optimization. For crystal structural optimization, all atomic positions were relaxed until the atomic forces were smaller than 10^{-3} eV/Å. The vibrational frequencies were obtained from normal mode analysis. The elements of the Hessian matrix were calculated from the DFT forces using the finite difference method with an atomic step size of 0.015 Å. The frequencies were then obtained as the square roots of the eigenvalues of the Hessian matrix.

3. Results and discussions

3.1. Low pressure H_2 adsorption isotherm at -196˚C

Figure 2a illustrates the H_2 adsorption isotherms at -196˚C, covering the pressure range from 0 to 1 bar, calculated using the aforementioned thermochemical model. The experimental data and the results from classical force-field-based GCMC simulations [27, 28, 39] are also included for comparison. Notably, the GCMC simulation that employs a meticulously parameterized many-body polarization force field can reasonably replicate the experimental H_2 uptake of the BDC-Mg-MOF-74 framework [28]. Conversely, the GCMC simulation using a simpler many-body polarization force field significantly overestimate the H_2 uptake [27]. This discrepancy raises concerns about the accuracy of predictions for the newly-proposed isoreticular DHF-MOF-74.

Although the multiple-site Langmuir model is quite simple and some approximations are made during the calculations of Gibbs free energies of adsorption, the host-guest interactions described by DFT-D3 based simulations are quite accurate. Consequently, the integrated approach yields a reasonable H_2 adsorption isotherm of the original framework at -196˚C within the pressure range of 0 to 1 bar. This integrated approach demonstrates a good agreement with the experiment and meticulously parameterized force-field based GCMC simulations especially in the low-pressure range below 0.1 bar. However, in higher pressure range, the uptake from our model appears to nearly reach saturation and then suddenly increases at 0.2 bar. In contrast, no saturation behavior is observed from either experiment data or GCMC simulations.

To gain insight into the factors contributing to this discrepancy, we analyze the site-specific coverage rates as illustrated in Fig. 2b. According to this, the coverage rate of PM site increases quickly and approaches saturation at 0.2 bar, while the coverage rates of the remaining sites are negligible. This behavior account for the near saturation observed in the adsorption isotherm. Meanwhile, the coverage rates of other sites increase much more slowly. The coverage rate of PO1 site becomes significant and increases linearly above 0.2 bar, resulting in the increase in slope of the isotherm at 0.2 bar. The coverage rates of PR and PO2 sites coincide and remain negligible

until 0.4 bar, at which point the adsorption isotherm is observed to start increasing linearly. At 1 bar, our model overestimates the uptake by 8%.

It is worth mentioning that, at this pressure, the coverage rate of PO1 exceeds 0.5, which is likely to significantly impact the adsorption energies of other sites. Moreover, as the PM sites are almost fully covered before the coverage rate of PO1 becomes considerable, we deem the influence of pre-occupied PO1 sites on PM sites to be negligible. Therefore, only the omission of PO1-PO1, PO1-PR and PO1-PO2 site-site interactions could be the primary cause of the overestimation of H_2 uptake at high pressure. Without H_2 adsorption at PR and PO2 sites, H_2 adsorption by PM sites gives reasonable shoulder of the H_2 adsorption isotherm at about 0.1 bar as shown in Fig. 2c. In higher pressure range up to 1 bar, the hydrogen uptake was underestimated by 4 % to 10 %. To produce a more accurate adsorption isotherm for higher pressure ranges, it is essential to include the effects of PO1-PO1, PO1-PR and PO1-PO2 site-site interactions.

The saturation coverage rate of the PM site in the newly-proposed framework is achieved at a lower pressure of 0.1 bar as compared to the original framework (Fig. 2d). This finding appears to contradict the predictions made by the previous DFT calculations, which indicated a lower adsorption energy at zero temperature for the PM site in the new framework (17.3 kJ/mol) compared to the original framework (18.5 kJ/mol) [34]. However, it is important to consider the contribution of vibrational, rotational and translation motions which can probably reverse the situation. In Fig. 3a, we present the evolutions of Gibbs free energies of adsorption for both PM and oxygen-related sites in the two frameworks as a function of temperature at a fixed pressure of 0.1 bar. It is evident that at temperatures below -170˚C, the PM site in the new framework exhibits a stronger affinity compared to the original framework, as indicated by a more negative Gibbs free energy of adsorption. The situation is reversed again at higher temperatures. This observation highlights that the adsorption energy at zero temperature alone is not the sole determining factor for evaluating the H_2 adsorption performance of an adsorption site. The effects of vibrational, rotational, and translational contributions must be taken into account to comprehensively assess the site's performance.

The evolutions of Gibbs free energies of adsorption for oxygen-related sites also exhibits similar behavior. Namely, below -170˚C, the oxygen-related site in the new framework demonstrates stronger affinity than that of the original framework, while at higher temperatures, the situation becomes reversed. Fig. 3b illustrates the changes in Gibbs free energies of adsorption for these sites as a function of pressure at a constant temperature of -196˚C. The plot clearly demonstrates that the adsorption sites within the DHF-Mg-MOF-74 framework exhibit greater strength compared to their counterparts in the BDC-Mg-MOF-74 framework across the entire range of considered pressures. Consequently, at the given temperature and pressure range, the coverage rate of the PO2 site in the new framework are higher than that of the PO1 site in the original framework, as observed from Fig. 2(b,d).

3.2. High pressure H_2 adsorption isotherm at temperatures between -40˚C and 60˚C

The working temperature range targeted by the DOE is from -40˚C to 60˚C. Before proceeding to analyze the high pressure adsorption isotherm at temperatures in this range, it is essential to acknowledge the validity of our thermochemical model. The model is only applicable when the coverage rates of secondary adsorption sites, namely, the PO1, PR and PO2 in the original

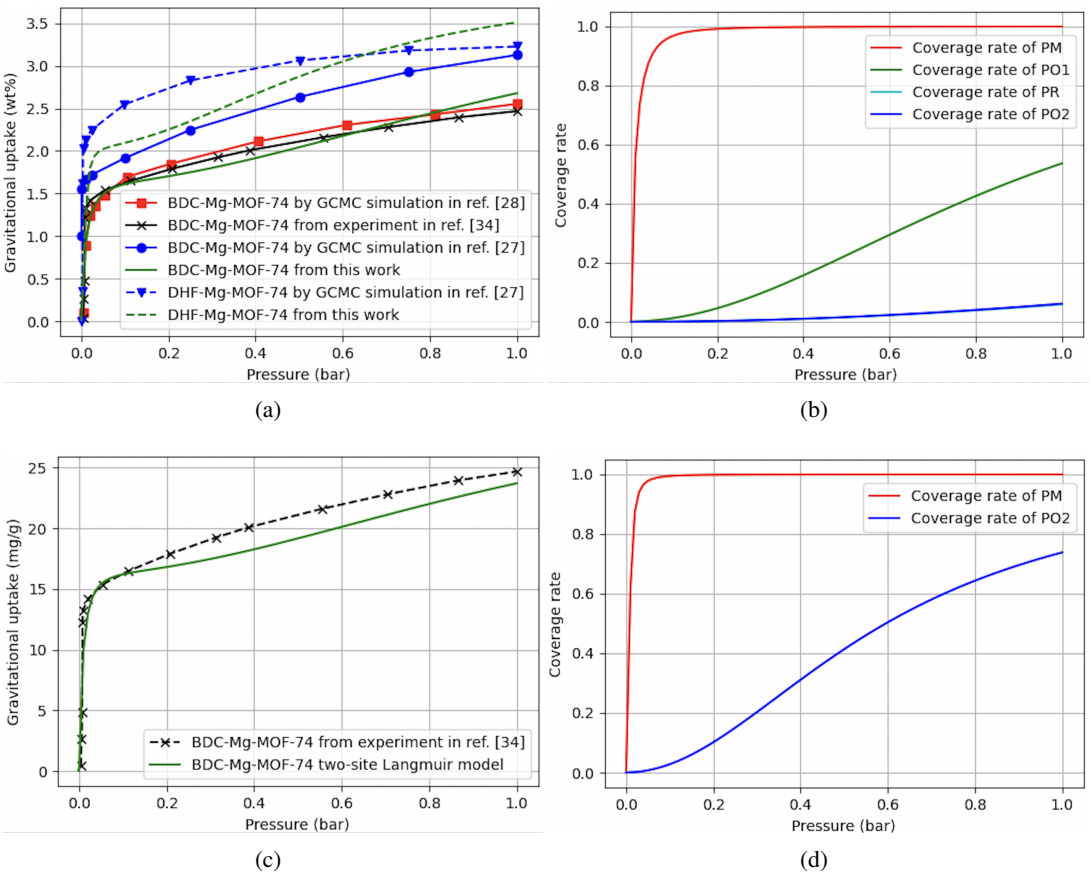

Fig. 2. (a) The H_2 adsorption isotherms of the Mg-MOF-74 isoreticulars at -196˚C, covering the pressure range from 0 to 1 bar from experimental data [39], GCMC simulations [27, 28] and calculated using our thermochemical model in which all adsorption sites are taken into account.
(b) The site-specific coverage rates of adsorption sites on the internal surface of the original BDC-Mg-MOF-74 framework.
(c) The H_2 adsorption isotherms of the original BDC-Mg-MOF-74 isoreticulars at -196˚C, covering the pressure range from 0 to 1 bar from experimental data [39], calculated using our thermochemical model in which only PM and PO1 sites are taken into account.
(d) The site-specific coverage rates of adsorption sites on the internal surface of the original DHF-Mg-MOF-74 framework.

BDC-Mg-MOF-74 framework and the PO2 in the newly-proposed DHF-Mg-MOF-74 framework, are significantly low.

Figure 4a presents the coverage rates of the PM and PO2 sites in the new framework as a function of pressure, ranging from 0 to 50 bar, at various temperatures within the targeted range. It is evident that the coverage rates decrease as the temperature increases and increase with pressure. Notably, at the lowest considered temperature of -40˚C, the coverage rate of PO2 remains

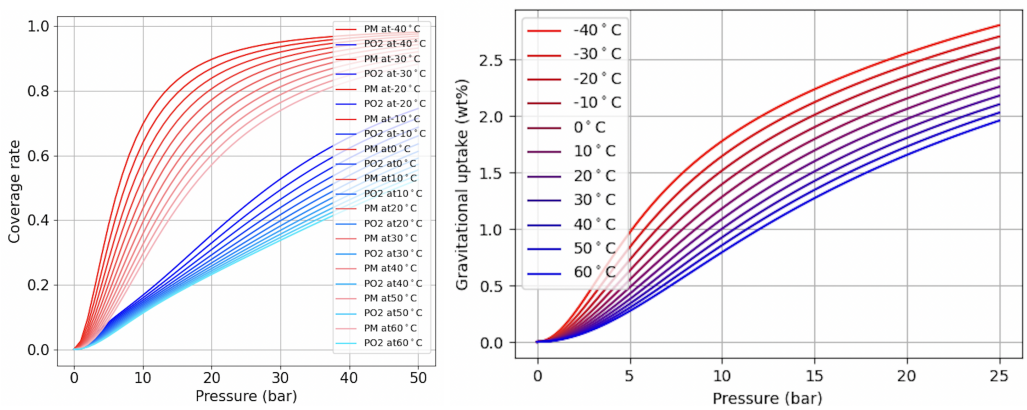

(a) (b)

Fig. 3. (a) The evolutions of Gibbs free energies of adsorption for the PM and oxygen-related sites in the Mg-MOF-74 isoreticulars as a function of temperature at a fixed pressure of 0.1 bar. (b) The evolutions of Gibbs free energies of the PM and oxygen-related sites in the Mg-MOF-74 isoreticulars as a function of pressure at a constant temperature of -196°C.

below 0.5 for pressures below 25 bar. Based on this observation, it can be inferred that our thermochemical model reliably predicts the adsorption isotherm of the DHF-Mg-MOF-74 framework within the pressure range below 25 bar at a specific temperature between -40°C and 60°C, as illustrated in Fig. 4b. This prediction highlights the much-improved H_2 adsorption performance of the newly-proposed DHF-MOF-74 isoreticular compared to its BDC linker-based counterparts. Specially, at a pressure of 25 bar, within a temperature swing from -40°C and 60°C, it can achieved a gravimetric hydrogen uptake value between 2.8 wt% and 1.9 wt%. In contrast, the experimental data of its BDC-linker-based counterparts show a much lower range, approximately from 0.3 wt% to 0.8 wt% [27].

When examining the original BDC-Mg-MOF-74 framework, under similar pressure and temperature conditions, the cumulative coverage rate of the secondary adsorption sites is comparable to the coverage rate of the PM sites, as depicted in Fig. 4c. Consequently, for the BDC-Mg-MOF-74 framework, the model tends to strongly overestimate the hydrogen uptake. Fig. 4d demonstrates the predicted adsorption isotherm which shows much better adsorption performance than its actual behaviour Witman2017.

4. Conclusion

In summary, a simple thermochemical model was developed on the based of the simplest model of adsorption proposed by Langmuir to calculate the H_2 adsorption isotherms of two Mg-MOF-74 isoreticulars. The model utilized adsorption energies and vibrational frequencies obtained from the DFT-D3 calculations as input variables. Although the model is relatively simple and employs certain approximations in calculating Gibbs free energies of adsorption, it is able to replicate the experimental H_2 adsorption isotherm of the original BDC-Mg-MOF-74 framework at

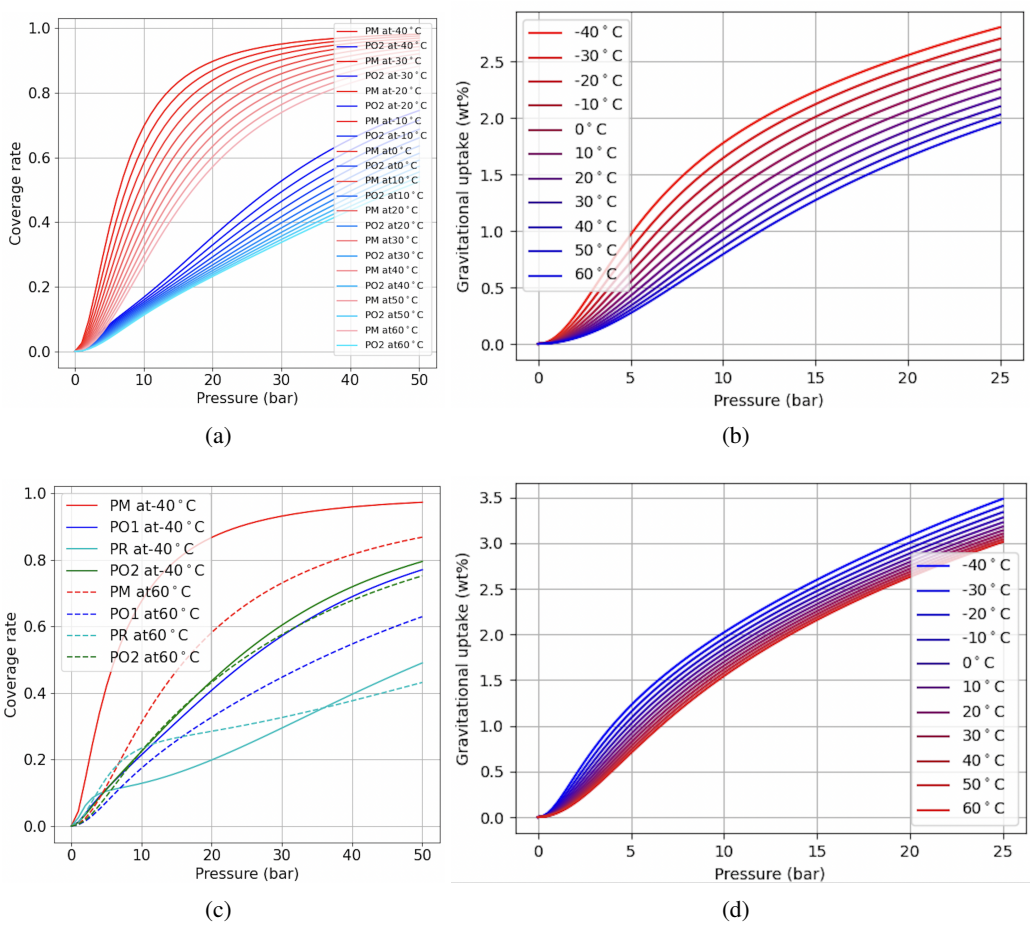

Fig. 4. (a) The coverage rates of the PM and PO2 sites in the DHF-Mg-MOF-74 framework as a function of pressure, ranging from 0 to 50 bar, at various temperatures between -40˚C and 60˚C.
(b) The H_2 adsorption isotherm of the DHF-Mg-MOF-74 framework within the pressure range below 25 bar at a specific temperature between -40˚C and 60˚C.
(c) The coverage rates of the PM, PO2, PR and PO2 sites in the BDC-Mg-MOF-74 framework as a function of pressure, ranging from 0 to 50 bar, at -40˚C and 60˚C.

-196˚C, within the pressure range up to 1 bar. Notably, it is predicted that the PM site of the new DHF-Mg-MOF-74 framework demonstrates saturation coverage rate at lower pressure compared to the original framework, despite a lower adsorption energy. This observation emphasizes that not only the H_2 adsorption energy but also the effects of vibration, rotational, and translational contributions must be taken into account for comprehensively assessing the site's performance. The validity of the model has been demonstrated when the coverage rates of secondary adsorption sites are low. Consequently, it tends to overestimate the H_2 uptake of the original framework at higher temperature and pressure ranges, where the cumulative coverage rate of the secondary

adsorption sites is high. Conversely, the model remains valid for the newly-proposed DHF-Mg-MOF-74 isoreticular within the temperature range from -40˚C to 60˚C and the pressure range up to 25 bar in which the coverage rate of the secondary adsorption site is less than 0.5. Its predictions highlight the substantially improved performance of the new framework compared to the original. Specially, it is capable of achieving a gravimetric hydrogen uptake value between 2.8 wt% and 1.9 wt% at a pressure of 25 bar within the mentioned temperature swing which is significantly higher than that of the original framework.

Acknowledgements

This research is funded by Vietnam National Foundation for Science and Technology Development (NAFOSTED) under grant number 103.01-2020.41.

Conflict of interest

The authors have no conflict of interest to declare.

References

[1] C. Weidenthaler and M. Felderhoff, *Solid-state hydrogen storage for mobile applications: Quo vadis?*, Energy Environ. Sci **4** (2011) 2495.

[2] R. Y. Sathe, T. J. D. Kumar and R. Ahuja, *Furtherance of the material-based hydrogen storage based on theory and experiments*, Int. J. Hydrog. Energy **48** (2023) 12767.

[3] The U.S. DRIVE Partnership, *Target explanation document: Onboard hydrogen storage for light-duty fuel cell vehicles*, 2017.

[4] J. Liu, Y. Ma, J. Yang, L. Sun, D. Guo and P. Xiao, *Recent advance of metal borohydrides for hydrogen storage*, Front. Chem. **10** (2022) 945208.

[5] T. Umegaki, J.-M. Yan, X. B. Zhang, H. Shioyama, N. Kuriyama and Q. Xu, *Boron- and nitrogen-based chemical hydrogen storage materials*, Int. J. Hydrog. Energy **34** (2009) 2303.

[6] H. Z. Liu, X. H. Wang, H. Zhou, S. C. Gao, H. W. Ge and S. Q. Li, *Improved hydrogen desorption properties of $LiBH_4$ by AlH_3 addition*, Int. J. Hydrog. Energy **41** (2016) 22118.

[7] H. Z. Liu, X. H. Wang, H. Zhou, S. C. Gao, H. W. Ge and S. Q. Li, *Hydrogen desorption kinetics of the destabilized $LiBH_4$-AlH_3 composites*, Int. J. Hydrog. Energy **42** (2017) 22358.

[8] S. Orimo, Y. Nakamori, T. Matsushima, T. Ichikawa, D. Chen and J. Gottwald, *Nanostructured carbon-related materials for hydrogen storage*, vol. XI, pp. 123–131, ASM International, 2002.

[9] J. J. Vajo, S. L. Skeith and F. Mertens, *Reversible storage of hydrogen in destabilized $LiBH_4$*, J. Phys. Chem. B **109** (2005) 3719.

[10] J. Weitkamp, M. Fritz and S. Ernst, *Zeolites as media for hydrogen storage*, Int. J. Hydrog. Energy **20** (1995) 967.

[11] T. Zhao, X. Ji, W. Jin, W. Yang and T. Li, *Hydrogen storage capacity of single-walled carbon nanotube prepared by a modified arc discharge*, Fuller. Nanotub. Carbon Nanostructures **25** (2017) 355.

[12] D. Silambarasan, V. Surya, K. Iyakutti, K. Asokan, V. Vasu and Y. Kawazoe, *Gamma(γ)-Ray irradiated multi-walled carbon nanotubes (MWCNTs) for hydrogen storage*, Appl. Surf. Sci. **418** (2017) 49.

[13] V. Tozzini and V. Pellegrini, *Prospects for hydrogen storage in graphene*, Phys. Chem. Chem. Phys. **15** (2013) 80.

[14] L. F. Wan, E. S. Cho, T. Marangoni, P. Shea, S. Kang and C. Rogers, *Edge-functionalized graphene nanoribbon encapsulation to enhance stability and control kinetics of hydrogen storage materials*, Chem. Mater. **31** (2019) 2960.

[15] M. Gaboardi, N. S. Amade, M. Aramini, C. Milanese, G. Magnani and S. Sanna, *Extending the hydrogen storage limit in fullerene*, Carbon **120** (2017) 77.

[16] M. Shi, L. Bi, X. Huang, Z. Meng, Y. Wang and Z. Yang, *Design of three-dimensional nanotube-fullerene-interconnected framework for hydrogen storage*, Appl. Surf. Sci. **534** (2020) 147606.

[17] S. Ghosh and J. K. Singh, *Hydrogen adsorption in pyridine bridged porphyrin-covalent organic framework*, Int. J. Hydrog. Energy **44** (2019) 1782.
[18] A. Deshmukh, T. N. M. Le, C.-C. Chiu and J.-L. Kuo, *DFT study on the H_2 storage properties of Sc-decorated covalent organic frameworks based on adamantane units*, J. Phys. Chem. C **122** (2018) 16853.
[19] L. Xia and Q. Liu, *Lithium doping on covalent organic framework-320 for enhancing hydrogen storage at ambient temperature*, J. Solid State Chem. **244** (2016) 1.
[20] H. Zhao, Y. Guan, H. Guo, R. Du and C. Yan, *Hydrogen storage capacity on Li-decorated covalent organic framework-1: a first-principles study*, Mater. Res. Express **7** (2020) 035506.
[21] S. P. She, S. S. Priya, K. Sudhakar and M. Tahir, *A review on current trends in potential use of metal-organic framework for hydrogen storage*, Int. J. Hydrog. Energy **46** (2021) 11782.
[22] A. Chibani, G. Mecheri, A. Dehane, S. Merouani and I. Ferhoune, *Performance improvement of adsorptive hydrogen storage on activated carbon: Effects of phase change material and inconstant mass flow rate*, J. Energy Storage **56** (2022) 105930.
[23] Z. Xuan, Z. Qingrong, Z. Guobin and Z. Weidong, *Adsorption equilibrium and charge/discharge characteristics of hydrogen on MOFs*, Cryogenics **112** (2020) 103121.
[24] C. M. Quine, H. L. Smith, C. C. Ahn, A. H.-. Zamudio, D. A. Boyd and B. Fultz, *Hydrogen adsorption and isotope mixing on copper-functionalized activated carbons*, J. Phys. Chem. C **126** (2022) 16579.
[25] D. Zhao, X. Wang, L. Yue, Y. He and B. Chen, *Porous metal–organic frameworks for hydrogen storage*, Chem. Commun. **58** (2022) 11059.
[26] M. T. Kapelewski, T. Runčevski, J. D. Tarver, H. Z. Jiang, K. E. Hurst, P. A. Parilla *et al.*, *Record high hydrogen storage capacity in the metal–organic framework ni2 (m-dobdc) at near-ambient temperatures*, Chemistry of materials **30** (2018) 8179.
[27] M. Witman, S. Ling, A. Gladysiak, K. C. Stylianou, B. Smit, B. Slater *et al.*, *Rational design of a low-cost, high-performance metal–organic framework for hydrogen storage and carbon capture*, J. Phys. Chem. C **121** (2017) 1171.
[28] T. Pham, K. A. Forrest, R. Banerjee, G. Orcajo, J. Eckert and B. Space, *Understanding the H_2 sorption trends in the M-MOF-74 Series (M = Mg, Ni, Co, Zn)*, J. Phys. Chem. C **119** (2015) 1078.
[29] R. Mercado, B. Vlaisavljevich, L.-C. Lin, K. Lee, Y. Lee, J. A. Mason *et al.*, *Force field development from periodic density functional theory calculations for gas separation applications using metal-organic frameworks*, J. Phys. Chem. C **120** (2016) 12590.
[30] T. Nguyen-Thuy, P. Le-Hoang, N. H. Vu, T. N.-M. Le, T. L. H. Doan, J.-L. Kuo *et al.*, *Hydrogen adsorption mechanism of MOF-74 metal–organic frameworks: an insight from first principles calculations*, RSC Adv. **10** (2020) 43940.
[31] I. Langmuir, *The adsorption of gases on plane surface of glass, mica and platinum*, J. Am. Chem. Soc. **40** (1998) 1361.
[32] D. A. McQuarrie and J. D. Simon, *Molecular thermodynamics*. University Science Books, USA, 1999.
[33] T. T. Nguyen, T. N.-M. Le, T. T. Nguyen, T. B. Phan and D. N.-. Manh, *H_2 physisorption in fluorinated MOF-74: The role of fluorine from the perspective of electronic structure calculations*, Int. J. Hydrog. Energy **48** (2023) 8997.
[34] T. N.-. Thuy, P. L.-. Hoang, N. H. Vu, T. N.-M. Le, T. L. H. Doan, J.-L. Kuo *et al.*, *Hydrogen adsorption mechanism of MOF-74 metal–organic frameworks: an insight from first principles calculations*, RSC Adv. **10** (2020) 43940.
[35] G. Kresse and J. Furthmüller, *Efficient iterative schemes for ab initio total-energy calculations using a plane-wave basis set*, Phys. Rev. B **54** (1996) 11169.
[36] G. Kresse and D. Joubert, *From ultrasoft pseudopotentials to the projector augmented-wave method*, Phys. Rev. B **59** (1999) 1758.
[37] J. P. Perdew, K. Burke and M. Ernzerhof, *Generalized gradient approximation made simple*, Phys. Rev. Lett. **77** (1996) 3865.
[38] P. E. Blöchl, *Projector augmented-wave method*, Phys. Rev. B **50** (1994) 17953.
[39] P. D. C. Dietzel, P. A. Georgiev, J. Eckert, R. Blom, T. Strässle and T. Unruh, *Interaction of hydrogen with accessible metal sites in the metal-organic frameworks m2(dhtp) (cpo-27-m; m = ni, co, mg)*, Chem. Commun. **46** (2010) 4962.